DOI: 10.1557/adv.2018.180

Density Functional Theory study of Cu doped {0001} and {01$\bar{1}$2} surfaces of hematite for water splitting

Joseph Simfukwe[1,2*], Refilwe Edwin Mapasha[1], Artur Braun[3] and Mmantsae Diale[1]

[1] *Department of Physics, University of Pretoria, Pretoria 0002, South Africa*

[2]*Department of Physics, Copperbelt University, Riverside, Kitwe 10101, Zambia*

[3]*Laboratory for High Performance Ceramics. Empa. Swiss Federal Laboratories for Materials Science and Technology, CH -8600 Dübendorf, Switzerland*

ABSTRACT

Density Functional Theory (DFT) calculations study of Cu doped {0001} and {01-12} surfaces of hematite for enhanced water splitting have been carried out. The doping was restricted to planes in the vicinity of the surface, specifically from the top most layers to the third inner layer of Fe atoms. Thermodynamic stabilities were evaluated based on surface energies and formation energies. The evaluation of thermodynamic stabilities (negative formation energy values) shows that the systems are thermodynamically stable which suggest that they can be synthesized in the laboratory under favorable conditions. Doping on the top most layer yields the energetically most favorable structure. The calculated charge density difference plots showed the concentration of charge mainly at the top of the surface (termination region), and this charge depleted from the Cu atom to the surrounding Fe and O atoms. This phenomenon (concentration of charge at the top of the surface) is likely to reduce the distance moved by the charge carriers, decrease in charge recombination leading to facile transfer of charge to the adsorbate and, suggesting improved photoelectrochemical water oxidation activity of hematite. The analysis of electron electronic structure reveals that Cu doped surface systems does not only decrease the band gap but also leads to the correct conduction band alignment for direct water splitting without external bias voltage.

INTRODUCTION

Increasing demand for sustainable clean (carbon free) energy is the motivation for the development of solar energy conversion technologies such as electrical power by photovoltaics (PV) and more recently again solar fuels by water splitting and Photoelectrochemical cells (PEC). In PEC water splitting, suitable semiconductors which can directly dissociate water molecules into hydrogen and oxygen species are needed.

Hematite (α-Fe_2O_3) possesses several advantages over other semiconductor materials for water splitting [1-5]. Its experimental band gap of ~ 2.1 eV allows it, to absorb about 40 % of the incident solar radiation [1, 2]. Hematite is also a very stable material in a broad pH range, non-toxic and abundant in the Earth's crust [3, 4]. These advantages have attracted a lot of research on hematite as a photoanode material for PEC. However, α-Fe_2O_3 also presents few challenges for its direct applications in PEC water splitting. Its conduction band which lies ~ 0.4 eV below that of H^+/H_2 redox potential [2, 3], does not favor the self-reduction of hydrogen. Practically, this means that an external bias is needed to drive this reaction. In addition, α-Fe_2O_3 suffers from low charge mobility (<1 $cm^2\ V^{-1}\ s^{-1}$) [3-5], fast electron-hole recombination rates (~10 ps) [6], and low surface reaction rates [3-5]. These shortcomings significantly limit full utilization of hematite for PEC applications. Various methods such as incorporation of dopants [7], creation of nanostructure α-Fe_2O_3 [8] with dopants and surface treatments [5, 6, 9, 10], have been employed to modify the photoactivity of α-Fe_2O_3. It is reported that bulk doping can improve the photocatalytic activity of α-Fe_2O_3, however, it also introduces localized impurities which can act as unwanted recombination centres for electron-hole pairs [9,12-14]. Effective doping requires the electron-holes to successfully diffuse to the surface and undergo interfacial charge transfer to the adsorbates [15]. Chang and Liu examined the effects of surface and bulk doping on the photocatalytic of vanadium (V)-doped TiO_2 based on charge trapping, separation and interfacial transfers [15, 16]. They found that the photocatalytic of the surface doped TiO_2 increased by 1.9 times compared to that of pure anatase. It is envisaged that surface doping is more beneficial than bulk doping because it reduces the distance moved by the charge carriers and further reduce quick recombination resulting in efficient use of the charges.

In this study, we derived the electronic structure of Cu doped {0001} and $\{01\bar{1}2\}$ surfaces of hematite for enhanced water splitting using density functional theory (DFT). The doping was restricted to the uppermost lattice planes specifically from the top most layers to the third inner layer of Fe atoms. The evaluation of thermodynamic stabilities shows that the systems are thermodynamically stable and suggests that they can be synthesized in the laboratory. The charge density difference plots showed the concentration of charge mainly at the top of the surface, which is the termination region.

This phenomenon (concentration of charges on top of the surface) is likely to reduce the distance moved by the charge carriers; decrease of premature charge recombination leading to facile transfer of charges (holes) to the adsorbed water molecules and consequently to improved PEC activity of hematite when it is doped in the way we assumed in our calculations. The results further show that Cu doped surface systems can both lower the band gap and lead to the correct conduction band alignment for direct water splitting without the external bias voltage. Meng *et al* [11] investigated Cu and Ti doped of bulk hematite with DFT +U for enhanced PEC, they also found that Cu doped bulk hematite moved the lower conduction band edge to high energy by about 0.5 eV leading to direct dissociation of water.

COMPUTATIONAL DETAILS

First-principles calculations were performed using the self consistent plane wave PWSCF code as implemented in quantum-espresso simulation package [17] based on the spin-polarized density functional theory (DFT) [18, 19]. The electronic exchange-correlation energy was treated within the generalized gradient approximation (GGA) parameterized by Perdew, Burke and Ernzerhof (PBE) [20]. The Utralsoft Pseudo potentials of PBE were employed for the electrons-ion interaction. The strongly

correlated electronic nature of the Fe 3d electrons was corrected with the coulomb correction in the frame work of GGA + U as applied by Duradev *et al* [21-23] with (U=5 eV). The Brillouin zone integration was sampled using Monkhorst-Pack scheme [24]. The k-point grids of 4x4x2 were employed for the structural relaxation of bulk unit cell, were as the k 12 x 12 x 6 mesh were employed in the calculation of the density of states (DOS). To study the effects of doping, a 2 x 2 x 1 supercell of {0001} and {01-12} surfaces with 120 atoms each was adopted. A k-point grids of 2 x 2 x 1 was used in structural relaxation calculations and 8 x 8 x 2 for DOS calculations. The plane-wave energy cut off was set to 350 eV. This truncation kinetic energy and the dense grids ensured accurate description of the properties and considered the calculation time cost. A vacuum spacing with a vertical distance of 20 Å was used to separate the electronic interaction between the periodic surface layers. Figure 1(a) show a hexagonal unit cell used to construct the surfaces and Table 1 gives a summary result of the structural and thermodynamic parameters of the bulk unit cell. Hematite has a hexagonal close-packed crystal structure with a space group $R\bar{3}c$ (No.167), containing six formula units (12 Fe and 18 O atoms). It is noted that two types of pairs of Fe atoms exist, which are identified by a short Fe-Fe distance (type A) and by a larger distance (type B) along the c hexagonal axis. Furthermore, along the c-axis, α-Fe_2O_3 is alternately stacked by iron and oxygen atom layers as can be seen in Figure 1(a). This makes it possible to construct either a Fe-layer terminated or O-layer terminated surfaces. In our calculations both terminations were constructed and analyzed by calculating their surface energies and other surface indexes were considered. Table 2 contains results of the calculated surface energies for various surfaces and compares them with other research results. Our results indicated that the single Fe-terminating {0001} was more stable as compared to the O-terminating surface and this compared very well with literature.

RESULTS AND DISCUSSION

Structural and electronic properties of pristine bulk hematite

In order to test our calculation methods, we started by carrying out the geometrical optimization of the pristine bulk α-Fe_2O_3 using PBE and PBE+U functionals. Table 1 summarizes the structural properties (*a* and *c*) and Fe-O bond lengths in (Å), thermodynamic stability (formation and cohesive energies) and the electronic properties (band gap). It can be seen that PBE calculation gives a smaller band gap compared to PBE+U calculation. In agreement with previous studies, PBE+U band gap is comparable to experimental value and previous theoretical calculations. As for the thermodynamic stability analysis, PBE gives formation and cohesive energies closer to the experimental values than PBE+U. This trend was also observed by Zhou *et al* [25]. The values inside the bracket are from the previous studies, while those outside are the calculated present work. Figure 1 (a) and (b) shows the band structure and the partial density of states (PDOS) respectively of pure hematite. It is clearly seen from PDOS that the valence band (VB) edge is mainly contributed by the O 2p states with a small contribution by the Fe 3d while the conduction band (CB) edge is dominated by the Fe 3d states. The results agree with experimental and previous theoretical results [5, 30]

Table 1: The Lattice constants (*a* and *c*) Å, Fe-O bond lengths (Å), formation and cohesive energies and band gap of pristine bulk α-Fe_2O_3 calculated using PBE and PBE+U functional.

	PBE	PBE + U	experiment
a (Å)	5.00 (5.01[13], 5.07[5])	5.13 (5.07 [13])	5.04[13, 26, 28]
c (Å)	13.85 (13.87[13], 13.88[5])	13.96 (13.90 [13])	13.75[13, 26]
Fe-O bond (Å)	1.93 (1.93[13], 1.97 [5])	1.99 (1.97 [13])	1.943[13, 26]
	2.13 (2.14 [13], 2.12 [5])	2.13 (2.12 [13])	2.11[13, 26]
Band gap (eV)	0.59 (0.52 [13], 0.57[25])	2.1 (2.15[13], 2.25[25])	2.0 – 2.2[13, 27]
Cohesive energy (eV)	-26.44 (-25.39 [25])	-22.76	-25.17[25]
Formation energy (eV)	-6.39 (-6.57 [25])	-2.72 (-4.71[25])	-8.56[25]

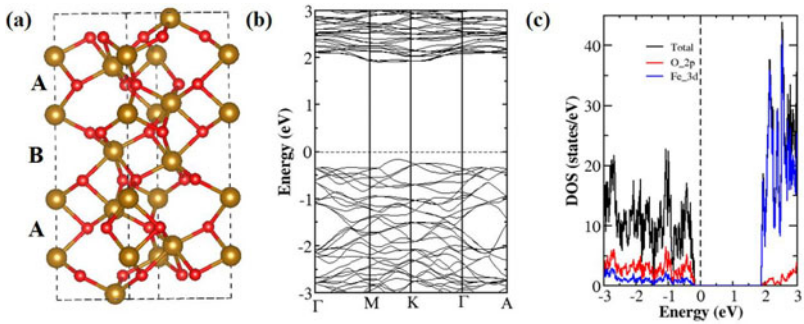

Figure 1. (a) Hexagonal closed-packed crystal structure of bulk hematite. The alternate stacking of Fe and O atoms are clearly shown. The two types of Fe pairs denoted as type A (short Fe-Fe distance) and type B (larger Fe-Fe distance) are also shown. Color scheme: Golden yellow (big spheres) and red (small spheres) represent Fe and O atoms respectively. (b) The band structure and (c) Total and partial density of electronics states (PDOS) of pure hematite. The Fermi level is set to zero.

Energetic Stability of few surfaces of α-Fe_2O_3

We constructed various surfaces of α-Fe_2O_3 presented in Table 2 and then determined their thermodynamic stability by calculating their surface (γ) and formation (E_f) energies. Comparing the thermodynamic stability of all the constructed surfaces, a low positive value of γ indicates the most stable surface. We calculated the surface energy γ using equation (1).

$$\gamma = \frac{1}{2A}(E_{slab} - n_{slab}\frac{E_{bulk}}{n_{bulk}}) \quad (1)$$

Where E_{slab} and E_{bulk} are the total energies of the slab and bulk respectively. n_{slab} and n_{bulk} are the corresponding number of atoms in these cells, A is the surface area of the slab cell and the factor ½ accounts for the two surfaces of the slab. If $n_{slab} = n_{bulk}$ then equation (1) becomes:

$$\gamma = \frac{1}{2A}(E_{slab} - E_{bulk}) \quad (2)$$

Formation energy calculations were done using equation (3):

$$E_f = E_{Fe_2O_3} - n_{Fe}\mu_{Fe} - n_O\mu_O \quad (3)$$

where E_{Fe2O3} *is* the total energy of the unit cell of the surface, n_{Fe} and n_O are numbers of Fe and O atoms in the unit cell respectively. μ_{Fe} is the chemical potential of α-Fe in its bulk structure, while μ_O is the chemical potential of O obtained from the O_2 place in a cubic box of 12 Å.The negative formation energy (E_f) implies that the formation of the surface is thermodynamically favourable [29]. Table 2 summarizes the results of both the surface and formation energies. It can be seen that the {0001} plane has two terminations, the Fe-termination and the O-termination. The Fe-termination is more stable than the O-termination. Our results compare very well with the theoretical results of previous results. It is also clearly seen that the {0001}-Fe and the {01-12} are the most stable surfaces. The Fe-termination surface energy is 1.84 J/m^2, while that of {01-12} surface is 1.44 J/m^2, which compares well with other previous results [30-33]. Our results showed that the {0001}-Fe and the {01-12} were the most energetically stable surfaces and so we focused our studies on these two surfaces.

Table 2: Calculated relaxed formation and surface energies of few surfaces of α-Fe_2O_3

Plane (hkil)	Formation energy (eV)	Surface energies (J/m^2)	
		Other works	This work
{0001} - Fe	-5.36	1.66[30], 1.78[31],1.53[32] ,2.31[31]	1.84
{0001} - O	-5.11	2.63[31], 2.59 [30]	2.80
{01-12}	-5.34	1.92[30], 1.88 [31], 1.47 [32]	1.44
{10-11}	-4.71	2.29[30], 2.34[31], 2.41[32] ,2.84[33]	2.56
{01-11}	-4.35	2.34[32]	1.97
{11-21}	-0.62	2.07[32]	2.20

Formation energy of doped α-Fe_2O_3 surfaces

Similarly, we determined the thermodynamic stability of Cu doped α-Fe_2O_3 surfaces by calculating the formation energy E_f *(Cu doped)* using equation (4) [13, 34].

$$E_f(Cu\ doped) = E(Cu\ doped) - E(pure) - \mu_{Cu} + \mu_{Fe} \quad (4)$$

where *E(Cu doped)* is the total energy of Cu doped surface; *E(pure)* is the total energy of the pure surface, μ_{Cu} and μ_{Fe} are chemical potentials of Cu and Fe respectively. The formation energies of the doped surfaces are allowed to vary as a function of the oxygen chemical potential μ_O, which stands for the growth conditions. These conditions could vary from O-rich (high value of μ_O) to Fe-rich (low value of μ_O). Therefore, the allowed values of μ_O and μ_{Fe} had to be determined first. For pure α-Fe_2O_3 in thermodynamic equilibrium μ_{Fe} and μ_O should satisfy equation (5) [13, 34].

$$2\mu_{Fe} + 3\mu_O = \mu_{Fe_2O_3} \quad (5)$$

Under Fe-rich conditions, the chemical potential μ_{Fe} was calculated from the energy of bulk body centred cubic (bbc) of α-Fe and the corresponding μ_O was evaluated from equation (5). Under O-rich conditions, the chemical potential μ_O was calculated from half of the energy of the O_2 molecule placed in a cubic box of 12 Å and the μ_{Fe} determined from equation (5). Figure 2 shows detailed structural description of what constitutes D1, D2 and D3 doped surfaces studied in this work. Table 3 summarizes the results of the formation energies of these doped surfaces under O-rich and Fe-rich conditions. The noted negative formation energies for the three doped layers (D1-D3) for both surfaces {0001} and {01-12} suggests that these material systems can easily be synthesized under favourable conditions. It is further observed that D1 of {0001} surface is the most favourable structure in both extreme conditions. It is evident that the reduction in co-ordination further lowers the energy of the system (D1) as opposed to D2 and D3 having complete co-ordination. For {01-12} surface, D2 is the most favoured structure with the most pronounced formation energy value under O-rich condition.

Table 3: Formation energies of Cu doped {0001} and {01-12} hematite surfaces calculated on the extreme conditions. The bold values indicate the most stable doped surface.

		Formation energy (eV)	
Plane (hkil)	**Doped layer**	**Fe-rich**	**O-rich**
{0001} - Fe	D1	**-3.42**	**-6.26**
	D 2	-2.89	-5.73
	D3	-2.77	-5.61
{01-12}	D1	-3.73	-6.28
	D2	**-4.47**	**-7.02**
	D3	-4.30	-6.86

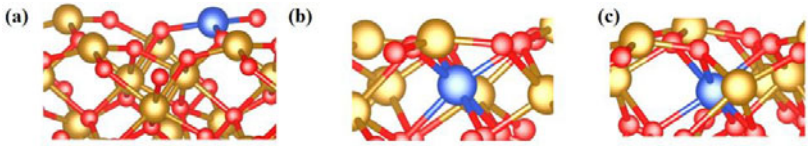

Figure 2. The relaxed doped surfaces. (a) The doped Cu atom (blue) on the top most layer of the {0001}-Fe terminating surface denoted as D1. (b) The doped Cu atom on the second layer of Fe atom denoted as D2. (c) The doped Cu atom on third layer of Fe atoms slightly below the second layer was denoted as D3.

Charge density difference

The charge density difference was plotted to understand the nature of charge distribution around the copper dopant. The charge density difference (ρ_{CDD}) is calculated using equation (6).

$$\rho_{CDD} = \rho_i^{total} - \sum \rho_i^{fragments} \quad (6)$$

where ρ_i^{total} is the total charge density of the Cu doped surface and $\rho_i^{fragments}$ is the charge density of the isolated pure surface and Cu atom. Figures 3 (a) and (b) show the top view and side view of (ρ_{CDD}) plots of D1 respectively. It is clearly noted that the charges are mainly concentrated at the top of the surface (termination region). Secondly, we find that most of the charge is depleted (represented by cyan colour) from the Cu atom shown by the cyan colour and accumulated (represented by yellow colour) on the neighbouring O and Fe atoms shown by the yellow colour. This observation is constantly seen in all the top surfaces not presented is this paper. The concentration of the charges on the surface is likely to decrease charge recombination and enable easy charge transfer to the adsorbates resulting in improved PEC.

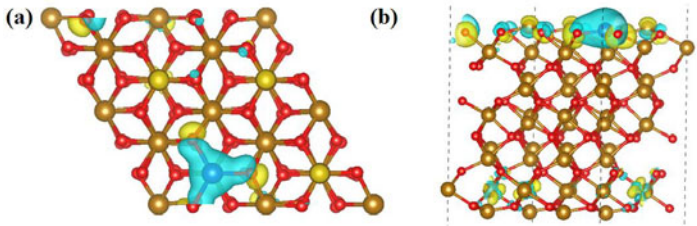

Figure 3. (a) Top and (b) side views of charge density difference of doped D1 surface calculated at the isosurface value of 0.03electrons/bohr^3. The cyan color indicates decrease in charge density while the yellow color indicates increase.

Electronic structure

To understand the influence of copper on the electronic properties of {0001} and {01-12} surfaces, the band structure and partial density of states (PDOS) are plotted and shown in Figure 4 and Figure 5. Figure 4 (a and b) show the band structure and PDOS of pure {0001} surface with a band gap of 2.1 eV, whereas (c and d) and (e and f) present those of D2 and D3 respectively. The band gap of D2 and D3 of {0001} surface

reduced from ~2.1 eV to 1.72 and 1.92 eV respectively. These reductions in the band gaps are likely to enhance more PEC activity by enabling more absorption photons in the visible light region. The band structures of Figure 4 show inward shifting of CBM to high energy levels at M and K symmetry k- points as compared to that of bulk hematite shown in Figure 1 (b). To quantify this energy shifting, the DOS for the bulk hematite, D1, D2 and D3 are plotted on the same scale as shown in Figure 4(g). It is found that the CB band of D2 and D3 of {0001} shifted up by 0.2 eV and 0.4 eV respectively. According to Hu *et al* [1] and Meng *et al* [11], these values are sufficient for spontaneous reduction of hydrogen on the doped surfaces. Figure 5 (a and b) show the band structure and PDOS of pure {01-12} surface whereas (c and d) and (e and f) present those of D2 and D3 respectively. It is interesting to note that in Figure 5 (c) and (f) the CBM of D2 and D3 becomes wavier and delocalised than that of pure bulk hematite shown in Figure 1 (b). Pan *et al* [5] observed a similar characteristic when they doped bulk hematite with Titanium (Ti) and suggested that the delocalization of the CBM indicated a better carrier transport in the system due to a relatively small electron mass as implied by the wavy nature of the CBM. They further pointed out that the relatively small electron mass is likely to cause the excited electrons to feasibly move to the surface and join the redox reaction. We also think that with the observed wavy nature of the CBM on the {01-12} surface coupled with the concentration of the charges on the surface as seen in Figure 3 (a) and (b) there is a likelihood of improved PEC on the {01-12} surface. It is also seen from Figure 5 (d) and (f) that the band gap decreased from 1.43 eV to about 1.0 eV.

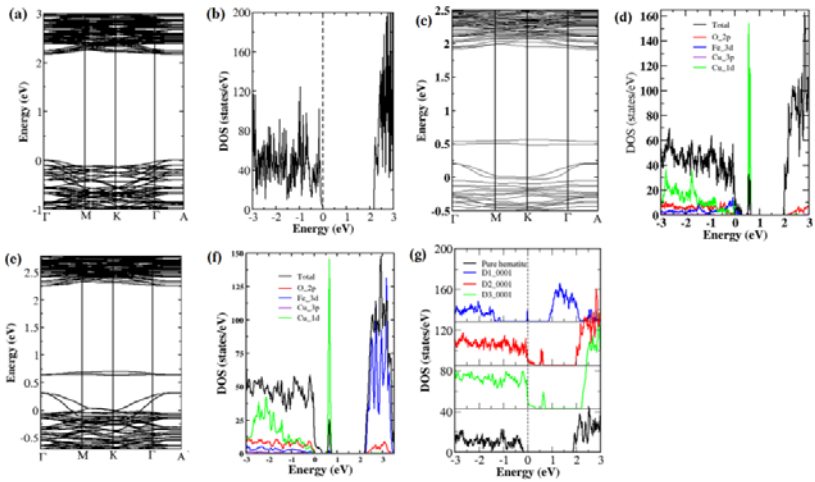

Figure 4. Band structure and density of states of pure {0001} surface (a) and (b), doped D2 (c) and (d), doped D3 (e) and (f) and DOS for the bulk hematite, D1, D2 and D3 are plotted on the same scale (g). The Fermi level is set to zero

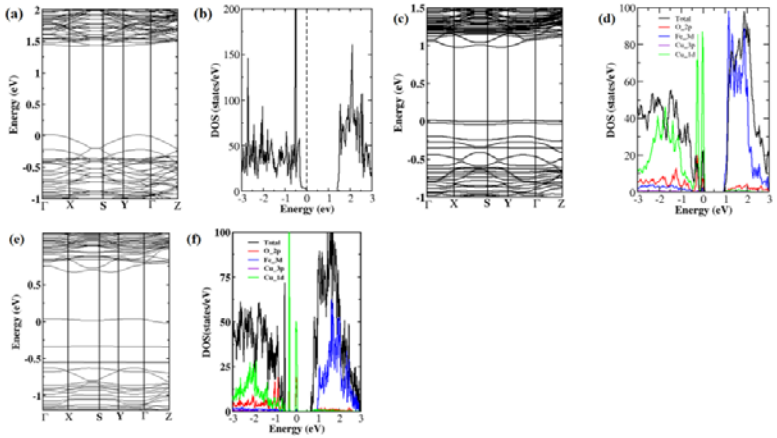

Figure 5. Band structure and density of states of pure {01-12} surface (a) and (b), doped D2 (c) and (d), doped D3 (e) and (f). The Fermi level is set to zero

CONCLUSION

In conclusion we have studied Cu doped {0001} and {01-12} α-Fe_2O_3 surfaces using first principles calculations. The doping was done at different layers of the surface, from the top most layers to the third inner layer of Fe atoms. We determined their thermodynamic stabilities based on surface and formation energies. As the systems are thermodynamically stable, it should be possible to synthesize them in the laboratory. Moreover doping on the top most layer yields the most energetically favorable structure. The calculated charge density difference plots showed the concentration of charge mainly at the top of the surface (termination region), and this charge depleted from Cu impurity to the surrounding Fe and O atoms. This phenomenon (concentration of charges on the surface) is likely to reduce the distance moved by the charge carriers; decrease of premature charge recombination leading to facile transfer of charges (holes) to the adsorbed water molecules and leading to improved PEC activity of hematite. The electronic structure analysis reveals that Cu doped surface systems can decrease the band gap and leads to the correct conduction band alignment for spontaneous water splitting.

ACKNOWLEDGMENTS

Dr. Richard Andrew (formerly at University of Pretoria and now at University of Johannesburg) is acknowledged for his initial guidance in the DFT. Thanks to the Copperbelt University for funding under the staff development fellowship fund. Further gratitude goes to the University of Pretoria and the Center for High Performance Computing (CHPC), Research Institute in Cape Town, South Africa for the cluster resources. AB and MD acknowledges financial support from the Swiss South African Joint Research Programme project "Production of Liquid Solar Fuels from CO_2 and water: Using Renewable Energy Resources" (IZLSZ2-149031). AB is grateful from the Swiss Nano Tera project SHINE (Solar Hydrogen Integrated Nano Electrolyzer, 20NA21-145936).

REFERENCES:

1. Y-S. Hu, A. K leiman-Shwarsctein, A. J. Forman, D. Hazen, J-N Park and E. W. McFarland, Chem. Matter, **20**, 3803 (2008)
2. M. Barroso, S. R. Pendlerbury, A. J. Cowan and J. R. Durrant, Chem. Sci., **4**, 2724 (2013)
3. H. J. Pan, X. Y. Meng and G. W. Qin, Phys.Chem. Chem. Phys, **16**, 25442 (2014).
4. J. A. Glasscock, P. R. F. Barnes, I. C. Plumb and N. Savvides, J. Phys. Chem. C,**111**, 16477-16488 (2007).
5. H. Pan, X. Meng, D. Liu, S. Li and G. Qin, Phys.Chem. Chem. Phys., **17**, 22179 (2015).
6. N. Mirbagheri, D. Wang, C. Peng, J. Wang, Q. Huang, C. Fan and E. E. Ferapontova, ACS Catalysis, **4,** 2006-2015 (2014).
7. J. J. Wang, Y. Hu, R. Toth, G. Fortunato, A. Braun, A facile nonpolar organic solution process of nanostructured hematite photoanode with efficiency and stability for splitting, J. Matter Chem A, **4**, 2821-2825 (2016).
8. F. Boudoire, R. Toth, J. Heier, A. Braun, E. C. Constable, Photonic light trapping in self-organized all-oxide microspheroids impacts on photoelectrochemical water splitting, Energy & Environmental Science, **7**, 2680-2688 (2014).
9. N. J. Cherepy, D. B. Liston, J. A. Lovejoy, H. M. Deng and J. Z. Zhang, J. Phys. Chem. B, **102**,770-776 (1998).
10. Y. Hu, F. Boudoire, I. Hermann-Geppert, P Bogdanoff, G. Tsekouras, B.S. Mun, G. Fortunato, M. Graetzel, A. Braun, Molecular Origin and Electrochemical Influence of Capacitance Surfaces States on Iron Oxide Photoanodes: The Journal of Physical Chemistry C, **120**, 3250-3258 (2016).
11. X. Y. Meng, G. W. Qin, S. Li, X. H. Wen, Y. P. Ren, W. L, Pei and L. Zuo, Applied Physics Letters, **98**, 112104 (2011).
12. R. Franking, L. S. Li, M. A. Lukowski, F. Meng, Y. Z. Tan, R. J. Hamers and S. Jin, Energy Environ. Sci, **6**, 500-512 (2013).
13. Z. Zhou, P. Huo, L. Guo and O. V. Prezhdo, J. Phy. Chem. C, **119**, 26303-26310 (2015).
14. S. Kumari, A. P. Singh, C. Tripathi, D. Chauhan, S. Dass, R. Shrivastav, V. Gupta, K. Screenivas and V. R. Satsangi, Int. J. Photoenergy, 87467 (2007).
15. S. Chang and W. Liu, Applied Catalysis B: Environmental, **101**,333-342 (2011).
16. K. Nagaveni, M. S. Hegde and G. Madras, J. Phys Chem. B, **108**, 20204-20212 (2004).
17. P. Giannozzi, S. Baroni, N. Bonini, M. Calandra, R. Car, C. Cavazzoni, D. Ceresoli, G.I. Chiarotti, M. Cococcioni, I. Dabo, A. Dal Corso, S. de Gironcoli, S. Fabris, G. Fratesi, R. Gebauer, U. Gerstmann, C. Gougoussis, A. Kokalj, M. Lazzeri, I. Martin-Samos, N. Marzari, F. Mauri, R. Mazzarello, S. Paolini, A. Pasquarello, I. Paulatto, C. Sbraccia, S. Scandolo, G. Sclauzero, A.P. Seitsonen, A. Smogunov, P. Umari, R.M. Wentzcovitch, J. Phys.: Condens. Matter **21**, 395502 (2009).
18. P. Hohenberg and W. Kohn, Phys. Rev, **136,** B864 (1964)
19. W. Kohn and L. J. Sham, Phys. Rev, **140,** A1133 (1965).
20. J. P. Perdew, K. Burke and M. Ernzerhof, Phys. Rev. Lett, **77,** 3865 (1996).
21. A. I. Liechtenstein, V. I. Anisimov and J. Zaanen, Phys. Rev. B **52**, R5467 (1995).
22. S. L. Dudarev, A. I. Liechtenstein, M. R. Castell, G. A. D. Briggs and A. P. Sutton, Phys. Rev. B **56**, 4900 (1997).
23. S. L. Dudarev, G. A. Botton, S.Y. Savrasov, C. J. Humphreys and A. P. Sutton, Phys. Rev. B **57**, 1505 (1998).
24. H. J. Monkhorst and J. D. Pack, Phys. Rev. B **13**, 5188 (1976).
25. Z. Zhou, J. Shi and L. Guo, Computational Materials Science, **113**, 117-122 (2016).
26. M. Catti, G. Valerio and R. Dovesi, Phys. Rev. B **51**, 7441-7450 (1995).
27. L. P. Liao and E. A. Carter, J. Phy. Chem. C, **13**, 15189-15199 (2011).
28. A. Rohrbach, J. Hafner and G. Kresse, Phys. Rev. B **70**, 125426 (2004).
29. P. Garg, S. Kumar, I. Choudhuri, A. Mahata and B. Pathak, J. Phys. Chem. C, **120**, 7052-7060 (2016).
30. N. Y. Dzade, A. Roldan and N. H. De Leeuw, Minerals, **4**, 89-115 (2014).
31. N. H. De Leeuw and T. G. Cooper, Geochim. Cosmochin. Acta, **71**, 1655-1673 (2007).
32. W. C. Mackrodt, Phys. Chem. Miner. **15**, 228-237 (1988).
33. N. J. Reeves and S. Mann, J. Chem. Soc. Faraday Trans. **87**, 3875-3880 (1991).
34. J. Wang, H. Sun, J. Huang, Q. Li and J. Yang, J. Phys. Chem. C, **118**, 7451-7457 (2014).